Analysis on Development of Magnetite Hollow Spheres through One-Pot Solvothermal Process

Dung T. Nguyen and Kyo-Seon Kim
Dept. of Chemical Engineering, Kangwon National University, Chuncheon, Kangwon-Do 200-701, Korea

DOI 10.1002/aic.14139
Published online June 17, 2013 in Wiley Online Library (wileyonlinelibrary.com)

Monodisperse magnetite nanospheres with hollow interior structure were synthesized through one-pot solvothermal process, in an isothermal environment at 200°C for 12 h, using a sole iron precursor ($FeCl_3.6H_2O$) and without any template. We demonstrated the development of hollow structure of magnetite spheres by characterizing systematically the changes of morphology and crystal structure for different processing times. We also provided the cross-sectional images of the Fe_3O_4 spheres at different processing times to visualize the hollowing process inside the spheres with time. A detailed process mechanism to form the hollow structure of magnetite spheres was proposed, combining the formation of numerous tiny grains, the spherical assembly of those grains and the chemical conversion of the Fe (III) compounds to generate Fe_3O_4 simultaneously coupled with the Ostwald ripening process within the magnetite spheres. © 2013 American Institute of Chemical Engineers *AIChE J*, 59: 3594–3600, 2013
Keywords: magnetite spheres, one-pot solvothermal process, hollow structures, porous structure, template-free, Ostwald ripening

Introduction

Magnetite nanoparticles are of great interest for researchers in biotechnology/biomedicine fields because of their various applications such as targeted drug delivery for antitumor therapy, hyperthermia treatment of cancer cells, enzymatic assays and activity agent for medical diagnostics.[1–5] These applications of nanoparticles demand the properties of specific and uniform particle size, shape, surface structure as well as strong magnetic properties. Recently, monodisperse magnetite hollow particles have emerged as an ideal candidate for biomedical applications, because they integrate their unique magnetic properties with the valuable characteristics of hollow structure including low density, high surface-to-volume ratio and, specifically, high capacity for encapsulating various chemicals such as drugs, proteins, and genetic materials.

Generally, the synthetic strategies for the magnetite hollow structures can be roughly categorized into two methods: template and template-free approaches. The template method involves the precipitation of precursors or shell materials onto the template surface through various chemical or physical interactions between the shell layer and core template, followed by a post-treatment to form compact shell and to selectively remove templates to obtain the hollow structure.[6] Caruso et al.[7] prepared the composite core–shell and hollow magnetite spheres by coating polystyrene template with a mixture of magnetite nanoparticles and polyelectrolytes in aqueous solution to make sequential multilayers. The thickness of the deposited multilayers was controlled by either the number of adsorption cycles performed or the polyelectrolyte interlayer separation between each nanoparticle layer. Another study reported the synthesis of mesoporous magnetite hollow spheres by a direct chemical adsorption/precipitation of Fe^{2+} precursor on carboxyl-functionalized polystyrene templates.[8] The hollow core diameter was mainly determined by the diameter of the polymer beads and the thickness of the magnetite shell layer was controlled by the concentration of the Fe precursor. Peng and Sun[9] controlled the oxidation of Fe template to synthesize Fe-Fe_3O_4 core/shell and Fe_3O_4 hollow nanoparticle. The Fe template itself was involved as a reactant in the synthesis of the Fe_3O_4 shell material and, thus, simultaneously played the role of structure-directing scaffold and precursor for the Fe_3O_4 shell. Even though the template method has been proven as very effective and versatile method to synthesize the hollow structure, it exhibits the difficulties in term of achieving high product yield, removing the template completely and refilling the hollow interior with functional species simultaneously. Other disadvantages are related to high cost and tedious synthetic procedures which have impeded the large-scale production.

Recently, one template-free method to prepare inorganic hollow interior nanostructure has been developed based on the oriented attachment of many primary nanoparticles and subsequent Ostwald ripening.[10] It was proposed for the first time in the synthesis of anatase phase TiO_2,[11] and then has been applied to synthesize various kinds of materials such as Cu_2O,[12] ZnO,[13] and SnO_2.[14] This method involves the formation of aggregates from many primary nanoparticles and the gradual outward migration of inner primary nanoparticles through a dissolution-relocation process. Liu et al.[15] prepared the magnetite hollow nanospheres from $FeCl_3 \cdot 6H_2O$ and anhydrous sodium acetate in ethylene glycol solution and

Correspondence concerning this article should be addressed to K-S Kim at kkyoseon@kangwon.ac.kr.

rationalized the spontaneous dissolution-relocation of the particle interiors by considering the different acetate chelation modes between the outer and inner particles. Similarly, Zhu et al.[16] synthesized the magnetite hollow spheres in the presence of ethylenediamine (EDA) and proposed that EDA acted as a surfactant in ethylene glycol solution to form a layer on the surface of Fe_3O_4 nanocrystals and induced the assembly those nanocrystals to form loose aggregates which were subjected to the Ostwald ripening for the formation of hollow structure. Hu et al.[17] used ammonium acetate as a structure-directing agent and proved that ammonium acetate could generate many bubbles inside solution which provided the heterogeneous nucleation center for newly formed nanoparticles to build aggregates and, thus, some bubbles were remaining in the interior of the aggregates. Since the driving force for the Ostwald ripening could be attributed to the intrinsic density variations inside the solid aggregates, the presence of bubbles could significantly accelerate the outward migration of inner nanoparticles to generate the hollow structure. Different ammonium compounds, including urea, ammonia and ammonia bicarbonate which could generate gas bubbles were applied to synthesize the hollow spheres.[17–19] This recent approach provides an effective protocol to prepare hollow structures with high versatility for adjusting the size and inner structure. The relatively high-reaction temperature of this system favors the particles with a high crystallinity and, thus, a high magnetization to be applied for biomaterial diagnostics and therapy.

Although the hollowing process could be explained by Ostwald ripening, it should be notified, based on the literature survey, that the initial growth stage of magnetite nanoparticles was not clearly elucidated. Questions about the hollowing development still remain, and more systematic studies are required to understand this intriguing process. Herein, we analyzed the generation and growth of Fe_3O_4 hollow spheres systematically by observing the changes of morphology and crystal structure for different processing times until the hollow structures of the Fe_3O_4 nanoparticles were fully developed. Ultra-high resolution SEM, TEM, XRD, FTIR and VSM measurements were conducted to characterize the evolution of magnetite Fe_3O_4 hollow particles. We also provided the cross-sectional images of Fe_3O_4 spheres for different processing times to visualize clearly the hollowing process inside the spheres.

Experimental Section

To investigate the formation mechanism of Fe_3O_4 hollow spheres, we explored the growth process by monitoring the morphology and crystal structure of the product particles collected for various processing times. Typically, a solution of ethylene glycol ($C_2H_4(OH)_2$, J. T. Baker, AR) containing 0.1 M of $FeCl_3{\cdot}6H_2O$ (Sigma-Aldrich, $\geq$98%) and 1 M of ammonium acetate (CH_3COONH_4 or NH_4Ac, Sigma, $\geq$98%) was well mixed and then transferred to a Teflon-lined autoclave cell. The autoclave cell was kept inside an oven of high temperature to guarantee the uniform temperature inside the cell. The temperature of solution inside the cell was maintained at 200°C for different processing times. After the scheduled processing time, the autoclave cell was cooled to room temperature by using tap water. The product particles were obtained by centrifuging and washing with ethanol and water for several times and then were dried in a vacuum oven at 60°C for 6 h before characterization.

The SEM measurements of surface and cross section of the product particles were carried out with a Hitachi S-4800 ultra-high resolution SEM equipment using a 15 kV electron beam with the resolution of 1 nm. The TEM images of those particles were taken by a JEOL JEM-2011 transmission electron microscope. Powder XRD patterns were recorded with a Philips X'Pert PRO MPD X-ray diffractometer using Cu Kα radiation ($\lambda = 1.54060$ Å, 40 kV, 30 mA). The samples were scanned in step of 0.017° in the 2θ range of 20–80°. The FTIR spectra were obtained with an EXCALIBER UMA-500 spectrophotometer by using KBr pellet method. The magnetic properties of the product particles were measured with a Lake Shore £7300 vibrating sample magnetometer.

Results and Discussion

The morphology and structure of the product particles obtained at 200°C in the oven for 12 h were investigated by SEM and TEM measurements as shown in Figure 1. Figure 1a shows a formation of a large quantity of spheres with an average diameter of 300 nm. From the magnified image (Figure 1b), it should be noticed that the spheres were composed of many smaller grains. Some broken spheres and many holes on the surface of particles were clearly observed, confirming the formation of particles with solid shell. The hollow structure of the product particles was observed by the TEM measurements as shown in Figures 1c and 1d. An intensive contrast between the black margin and the bright center of the particles indicates the existence of hollow structure in the resulting spheres. Figures 1c and 1d reveal that the particles were of uniform hollow spheres with the average shell thickness of 40 nm from TEM measurements.

We investigated the changes of particle morphology and structure for different processing times by SEM measurements as shown in Figure 2. The SEM image of particles after 0.5 h (Figure 2a) presents a sand-like bulk morphology compactly packed by numerous tiny grains, while the SEM image of product particles after 1 h (Figure 2b) shows the seaweed-like bulk morphology with many tiny grains. We could find a sudden emergence of rough spherical particles with uniform diameter of about 300 nm, mainly around the leaf edges of the seaweed-like bulk morphology. Inset of Figure 2b indicates that the spherical particles were formed with the assembly of many tiny grains. The following samples at 3 h and 6 h showed an increase in the number of spherical particles. After 8 h (Figure 2e), clear large-sized spheres without sand-like grain matrix were observed, which means all grains have transformed into the large-sized spheres. The SEM image of particles obtained after 10 h (Figure 2f) shows the formation of a large amount of regular spheres with high uniformity. Some spheres with many holes on the surface were clearly observed after 10 h.

Figure 3 shows the XRD patterns of the product particles synthesized at 200°C for various processing times. The XRD diffraction peaks of particles obtained at 200°C after 12 h are shown in Figure 3g and can be well indexed to the faced-center cubic structure of Fe_3O_4 (reference code: 01–088-0315) with lattice constants of 8.375 Å. No peak corresponding to the hematite or other impurities was detected, indicating the formation of pure magnetite products. It should be noticed that the particles obtained for 0.5 h showed poor crystallinity and no XRD peak was observed. Along with the formation of spheres, the XRD peaks at $2\theta = 35.49°$

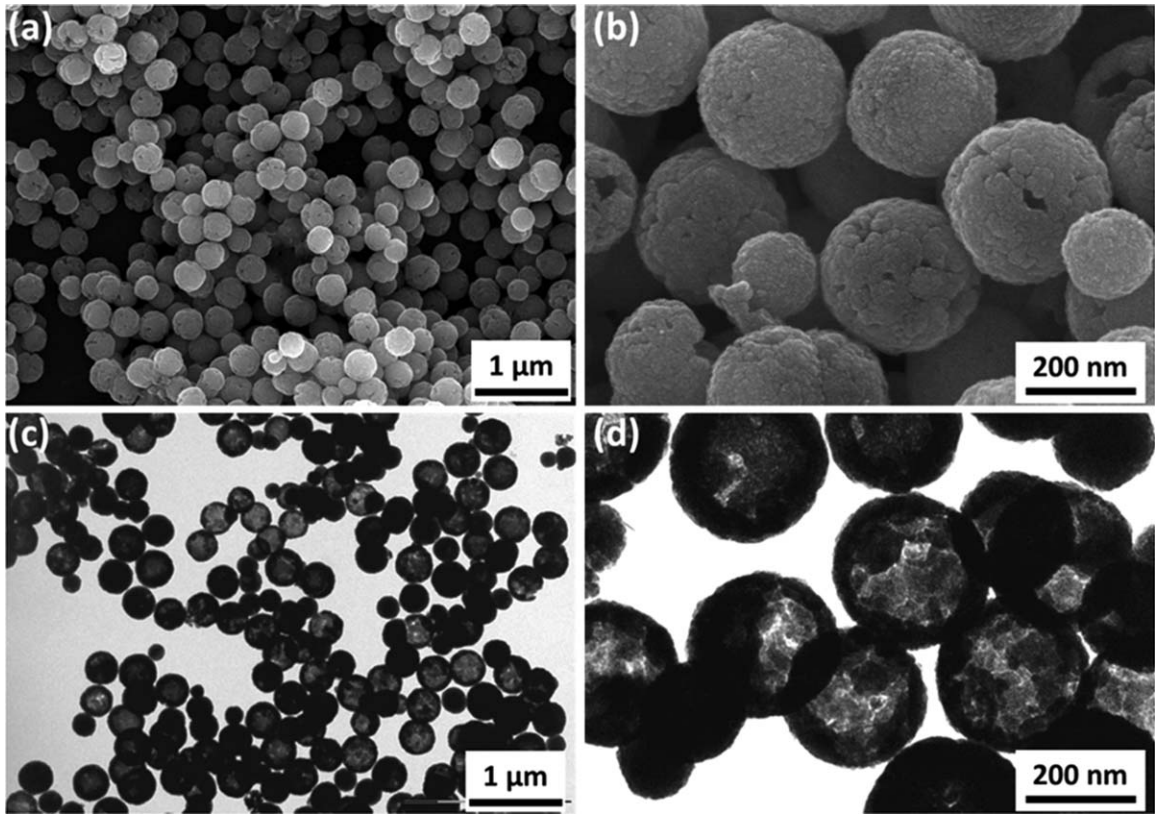

Figure 1. Representative (a,b) SEM and (c,d) TEM images of the magnetic nanoparticles prepared for 12 h in oven at 200°C.

corresponding to the (311) face of the magnetite appeared after 1 h of the processing time. The increase of processing time led to the appearance of the XRD peaks at $2\theta = 30.13$, 43.16, 57.04, and 62.64° corresponding to the (220), (400), (511) and (440) faces of Fe_3O_4 structures, respectively. These peaks became sharper with the increase of processing time and all peaks were clearly observed after 8 h.

Figure 4 presents the FTIR spectra of particles prepared for different processing times. Samples obtained until 6 h showed the gradually reduced absorption peaks at 1576 cm^{-1}, 1445 cm^{-1} and 1089 cm^{-1} with time due to asymmetric, symmetric stretching of the COO— group and C—O stretching of the COO— group, respectively.[20] Several peaks below 800 cm^{-1} are attributed to Fe-O modes due to the mixed phase of Fe compounds.[21,22] The peak at 530 cm^{-1} is assigned to the hydroxyl-bridge of Fe—OH.[21,22] These indicate that chloride (—Cl) groups in iron precursors were substituted after 0.5 h by hydroxyl (—OH) and acetate (—Ac) groups which have higher affinities to Fe (III) ions than chloride to give a precipitate. Some water molecules which were derived from Fe precursor ($FeCl_3 \cdot 6H_2O$) might adsorb on the precipitate grains and act as the binder for the further assembly between grains to form the large-sized spheres.[23] After 8 h, the peaks corresponding to acetate groups faded away and became difficult to be recognized. The peak at nearly 584 cm^{-1} due to the Fe—O lattice mode of Fe_3O_4 appeared and was gradually sharpened with time.[24] Along with the disappearance of acetate bands with time, we observed visually that the color of product particles changed from brown (before 1 h) to brownish black (3 h, 6 h), and finally to black (from 8 h) during the experiments. A brown precipitate which was observed before 1 h implied that the samples dominantly consisted of Fe (III) coordinated acetate compounds which are generally denoted here as $Fe(Ac)_x(OH)_{3-x}$ (with $x = 1-3$). The color change from brown to black implied the increase of newly formed magnetite. The amount of magnetite phase gradually increased and caused the darkening of the precipitates. Finally, the pure black precipitant implied the predominance of the magnetite phase which was consistent with XRD and FTIR measurements.

Magnetic measurements of the magnetite nanoparticles prepared for different processing times are shown in Figure 5. After 0.5 h, the precipitate responded very weak to an applied field with a weak magnetization saturation of about 2 emu g^{-1}, which means that just a small amount of magnetite particles exists. The magnetization saturation increased with time, consistent with the formation of more magnetite. A typical hysteresis loop was observed for all samples after 1 h, indicating a ferromagnetic behavior at room temperature. After 12 h, the hollow spheres showed a saturation magnetization of 81 emu g^{-1}, a remanent magnetization of about 22 emu g^{-1} and coercivity of about 200 Oe. The assembly of numerous small grains into hollow spheres built a multidomain structure of hollow spheres and, thus, caused the ferromagnetic behavior. The saturation magnetization of 81 emu g^{-1} here is high enough for particles to be easily manipulated by an external magnetic field and to be widely applied to cancer cell diagnosis and treatment.

Figure 6 shows the TEM images of product particles in the left-hand side and the corresponding SEM images of their cross-sectional structures in the right-hand side, respectively, for different processing times. To observe the cross-sectional structures of the magnetite particles for different processing times, the particles obtained were dispersed in

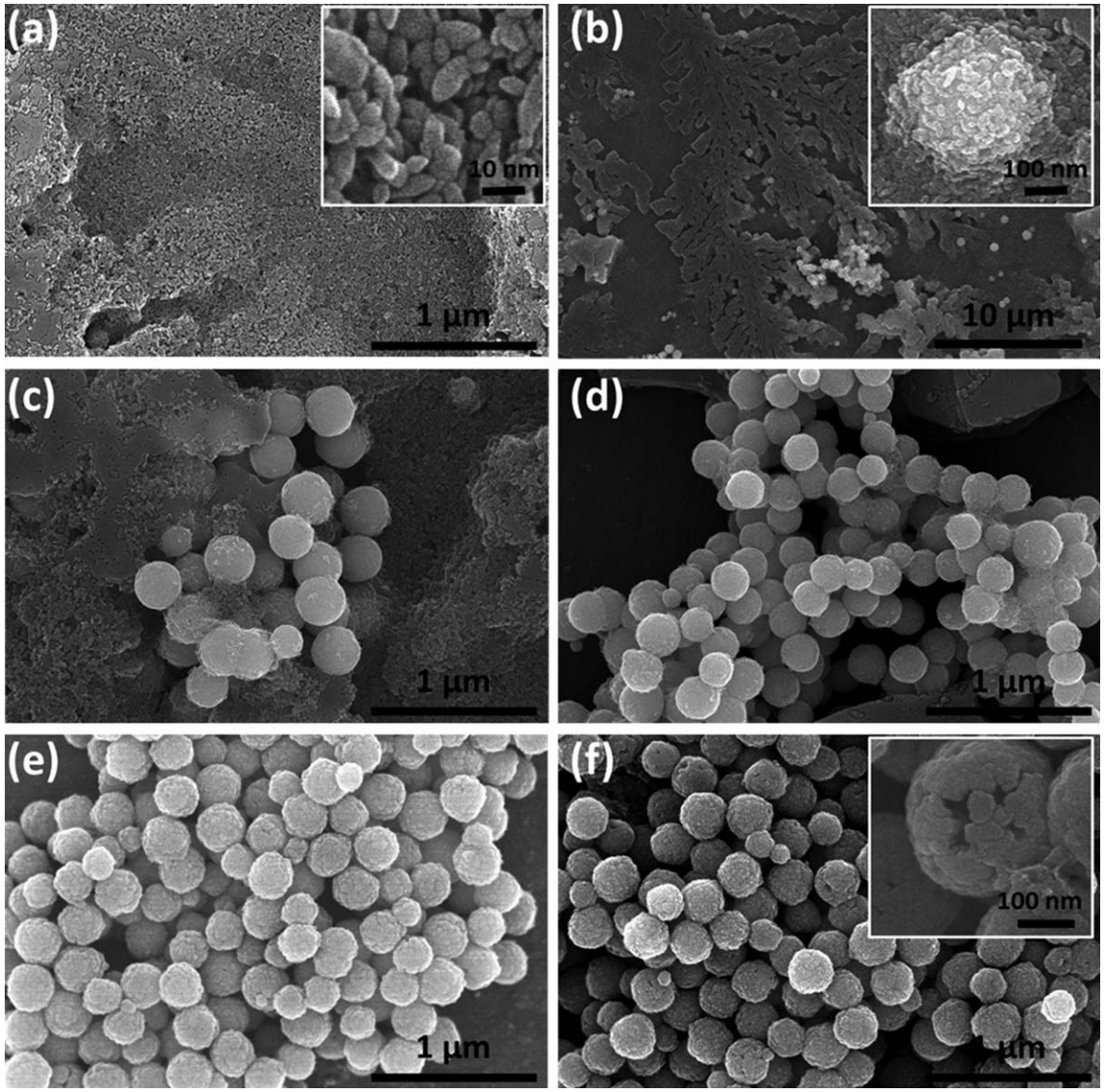

Figure 2. Representative SEM images of the product particles prepared for (a) 0.5 h, (b) 1 h, (c) 3 h, (d) 6 h, (e) 8 h, and (f) 10 h in oven at 200°C.

Insets in parts (a), (b) and (f) show the magnified SEM images of typical particles obtained after 0.5 h, 1 h and 10 h, respectively.

epoxy molds and then the epoxy molds were polished by diamond paper until the cross-sectional structures were exposed. The TEM and SEM images show the obvious changes of surface morphology and interior cavity of the particles with processing time. From Figure 6a and 6b, it seems that spherical particles with a compact core were obtained for the processing time of 6 h. The spheres were then followed by a solid core evacuation when the processing time increased. Many small cavities appeared inside for the spheres obtained after 8 h (Figure 6d). The hollowing effect was clearly observed for those spheres with a longer processing time of 10 h (Figures 6e and 6f). The cavities merged together and occupied the central core. The inner space of the spheres increased further when the reaction time was prolonged to 12 h (Figures 6 g and 6 h), indicating a continuous expansion of the central empty core. After 12 h, the hollow structure was well developed, but some small cavities were still trapped inside the solid shell, making the shell structure porous. It should be noticed that the hollowing process took place simultaneously with the chemical conversion process which was indicated by the intensive changes of XRD and FTIR data in Figures 3 and 4.

From all aforementioned observations, the formation mechanism of the magnetite hollow particles was proposed as shown in Figure 7. The formation mechanism comprised several different steps including the generation of sand-like bulk morphology compactly packed by numerous tiny grains, the formation of spherical particles by gathering of many small grains and the development of hollow structure based on the chemical conversion simultaneously coupled with the Ostwald ripening process. First, Fe (III) chloride reacted with ammonium acetate to give a sand-like precipitate of $Fe(Ac)_x(OH)_{3-x}$ as shown in Eq. 1

$$FeCl_3 \cdot 6H_2O + xNH_4Ac \rightarrow Fe(Ac)_x(OH)_{3-x} + xNH_4Cl + (3\text{-}x)HCl + (3+x)H_2O \quad (1)$$

Due to the interactions between bulk material and solution, the sand-like bulk materials were transformed into the

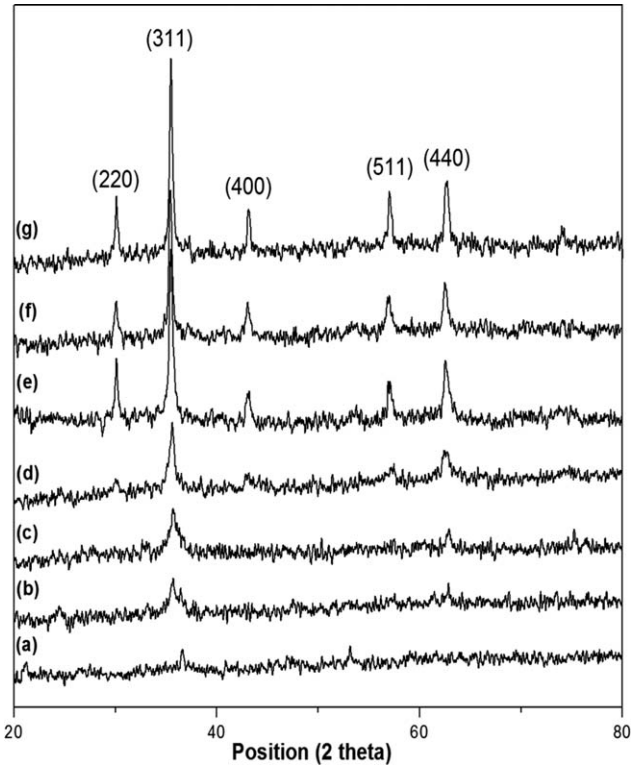

Figure 3. XRD patterns of the product particles prepared for (a) 0.5 h, (b) 1 h, (c) 3 h, (d) 6 h, (e) 8 h, (f) 10 h, and (g) 12 h in oven at 200°C.

seaweed-like bulk and, specifically, at the edge of the seaweed-like bulk, the assembly of tiny grains was gradually separated from the bulk material and then suspended into the ethylene glycol medium. The high viscosity of ethylene glycol solvent allowed the tiny grains to find the lowest energy configuration interface and assemble to become spherical particles with uniform size.[18,23] Our observation was consistent with previous studies on the formation of spherical aggregations of metal oxide nanoparticles in nonaqueous solution.[11–13] The particle size and morphology of the spheres mainly depended on the properties of solvents.[18,25]

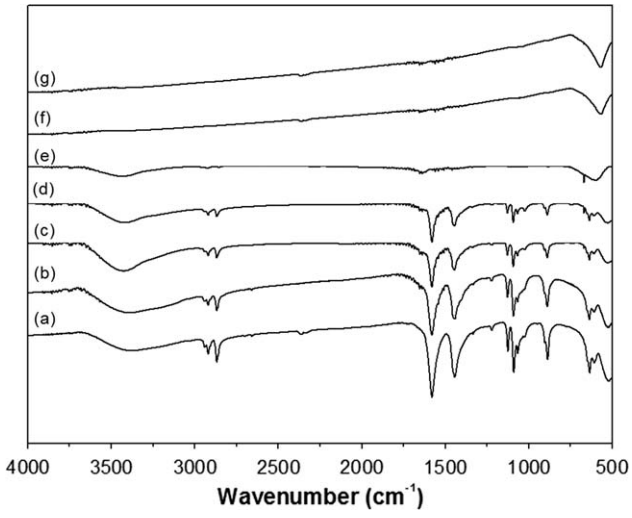

Figure 4. FTIR spectra of the product particles prepared for (a) 0.5 h, (b) 1 h, (c) 3 h, (d) 6 h, (e) 8 h, (f) 10 h, and (g) 12 h in oven at 200°C.

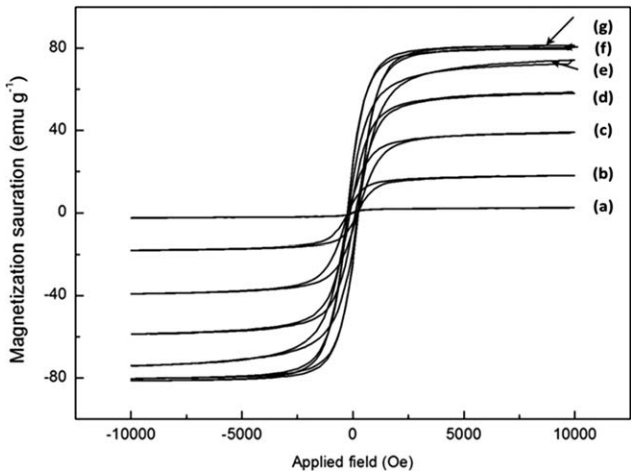

Figure 5. Room-temperature magnetization curves of the product particles prepared for (a) 0.5 h, (b) 1 h, (c) 3 h, (d) 6 h, (e) 8 h, (f) 10 h, and (g) 12 h in oven at 200°C.

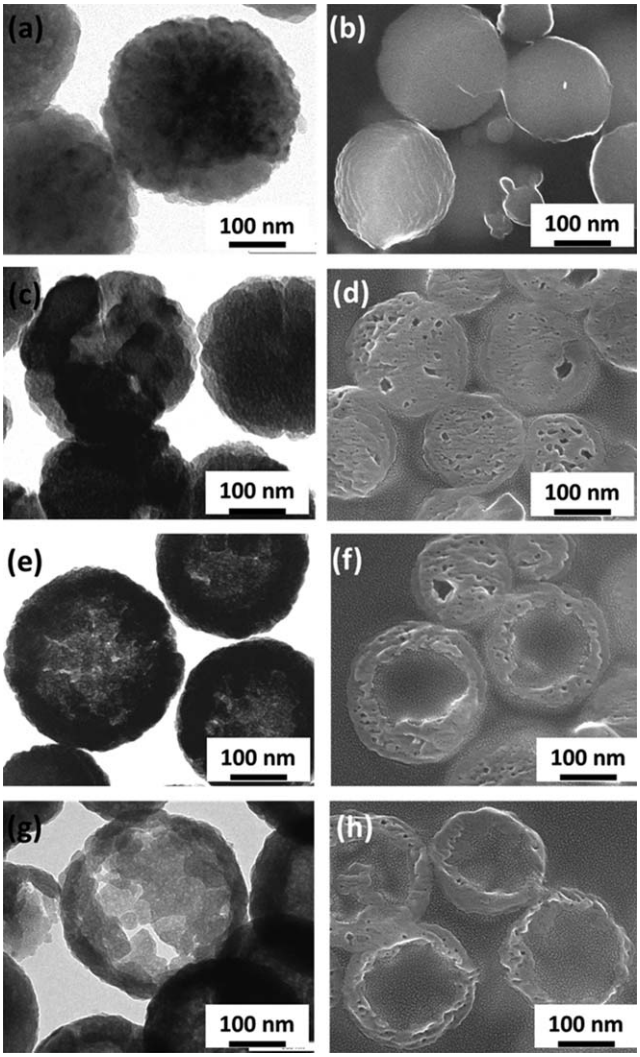

Figure 6. TEM images and corresponding cross-sectional SEM images of the product particles prepared for (a, b) 6 h, (c, d) 8 h, (e, f) 10 h, and (g, h) 12 h in oven at 200°C, respectively.

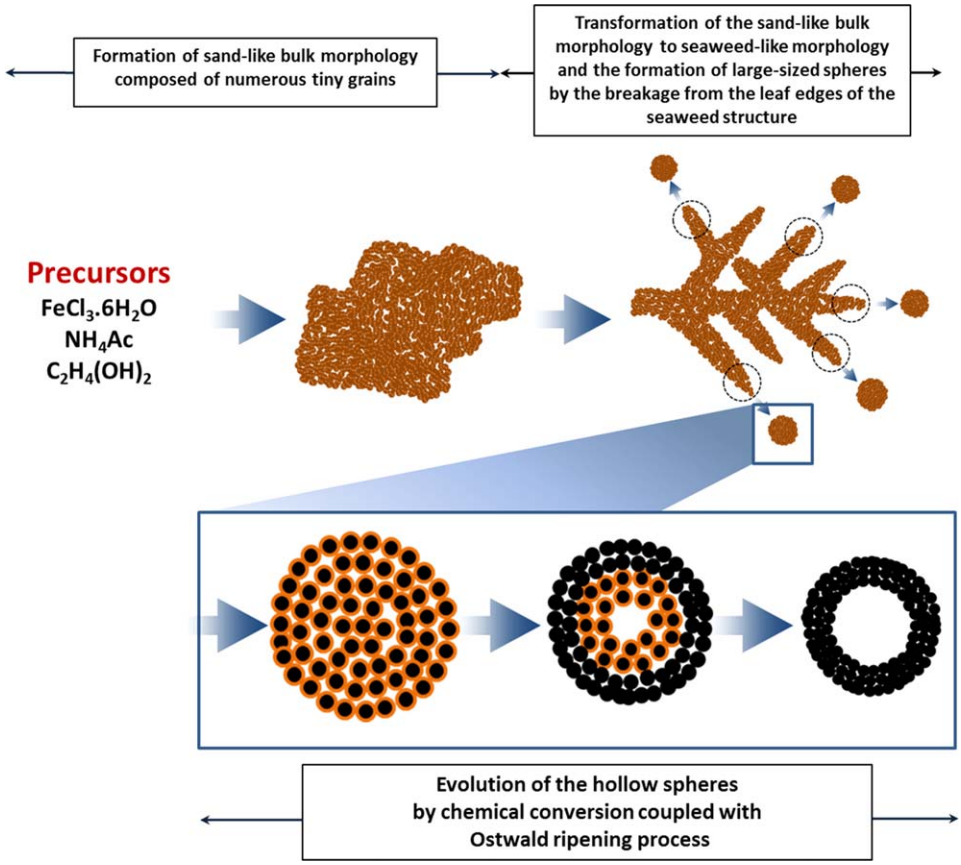

Figure 7. Schematic of the particle formation and the hollow structure development in solvothermal process.

[Color figure can be viewed in the online issue, which is available at wileyonlinelibrary.com]

We believe that the chemical conversion processes such as partial reduction reaction of the $Fe(Ac)_x(OH)_{3-x}$ compounds to generate the Fe (II) compounds (denoted as $Fe(Ac)_y(OH)_{2-y}$ with $y = 1–2$ and $y \leq x$) and subsequent hydrolysis and dehydrolysis reactions of those Fe (III) and Fe (II) compounds at elevated temperature should be involved to form the Fe_3O_4 nanoparticles.[15,18] The plausible chemical reactions involved in this process can be summarized as follows

$$2Fe(Ac)_x(OH)_{3-x} + 2C_2H_4(OH)_2 \rightarrow 2Fe(Ac)_y(OH)_{2-y} + CH_3COCOCH_3 + (4+2y-2x)H_2O + (2x-2y)HAc \quad (2)$$

$$Fe(Ac)_x(OH)_{3-x} + xH_2O \rightarrow Fe(OH)_3 + xHAc \quad (3)$$

$$Fe(Ac)_y(OH)_{2-y} + yH_2O \rightarrow Fe(OH)_2 + yHAc \quad (4)$$

$$2Fe(OH)_3 + Fe(HO)_2 \rightarrow Fe_3O_4 + 4H_2O \quad (5)$$

Water involved with the hydrolysis reactions 3 and 4, could be derived from $FeCl_3.6H_2O$ and be generated from the decomposition of ammonium acetate[26] ($NH_4OOCCH_3 \rightarrow NH_2COCH_3 + H_2O$) and also by the aforementioned chemical reactions 2 and 5. The water molecules generated by the chemical reactions 2 and 5 were not enough to make these hydrolysis reactions complete and some water molecules should be supplied to the spherical particles by diffusion from the ethylene glycol solution. The chemical reactions 2–5, therefore, took place progressively from the particle surface and to the core, leaving behind the converted materials.

Since the formation of hollow structure occurred simultaneously with the chemical conversion of solid material, we believed that the chemical conversion should be accounted as an important factor for the hollowing process. The chemical conversions from $Fe(Ac)_x(OH)_{3-x}$ to $Fe(OH)_3$, $Fe(OH)_2$, and Fe_3O_4 caused a little shrinkage of the grain size and thus made more voids between the grains inside the spheres. Those reduced grains around the exterior surface of spheres tended to shrink inward to make more stable and dense structures of grains and robust surface of spheres. However, the outer grains could not shrink inward any more after certain shrinkage, because the reduced grains become to have the compact structures between grains, and they become the exterior surface of solid shell spheres. Continuous chemical conversion process for inner grains would also make a little shrinkage of the grain size and more voids between grains and lead to the formation of loose package of grains. According to the Gibbs-Thompson equation and Fick's first law, the chemical potential of particle increases with the decrease in particle size, meaning that the equilibrium solute concentration surrounding a small particle would be higher than that surrounding a larger one. The resulting concentration gradients would lead to the diffusion of molecular-scale species from smaller particles to larger particles through solution.[27,28] The diffusion of solute component was quite important for the Ostwald ripening process to develop the hollow structure. For the hollow spheres with an average particle diameter of about 300 nm and shell thickness of about 40 nm, the diffusion distance would be 110 nm from the center to the inner surface of shell. Considering the

solubility of inner reduced grains and the diffusivity of solutes at the high processing temperature of 200°C for the relatively long processing time of 12 h, the inner grains would dissolve into the solution and then diffuse to the outer stable shell for the nanoscale diffusion distance by the Ostwald ripening process. The outward migration of the inner grains would result in continuous expansion of cavity space inside the spherical particles. Finally, the hollow structure was well developed with the complete chemical conversions of core grains.

Conclusions

The magnetite hollow spheres with the average diameter of 300 nm and the shell thickness of 40 nm were successfully synthesized through one-pot solvothermal process without any surfactant and template in an isothermal oven at 200°C for 12 h. Those particles were ferromagnetic with a high saturation magnetization of 81 emu g^{-1}. The formation mechanism of the magnetite hollow spheres comprised simultaneous chemical and physical processes including the formation of numerous tiny grains, the spherical assembly of those grains and the chemical conversion coupled with the relocation of the grains. The chemical conversion including a partially reductive reaction of the Fe (III) compounds and subsequent hydrolysis and dehydrolysis reactions of the Fe (III) and Fe (II) compounds to generate Fe_3O_4 caused the nonuniformities of tiny grains and the empty spaces within the spherical assemblies and thus enhanced the outward migration and relocation of the core grains toward the outer layer, resulting in the formation and expansion of the hollow core structure. We believe similar analysis can be extended for the development of hollow sphere structures with different precursors by the solvothermal process.

Acknowledgment

Following are results of a study on the "Leaders in Industry-University Cooperation" project, supported by the Ministry of Education, Science and Technology (MEST), and the National Research Foundation of Korea (NRF). Instrumental analysis was supported from the central laboratory of Kangwon National University.

Literature Cited

1. Kumar CSSR, Mohammad F. Magnetic nanomaterials for hyperthermia-based therapy and controlled drug delivery. *Adv Drug Deliv Rev*. 2011;63:789–808.
2. Nguyen DT, Park D-W, Kim K—S. Seed-mediated synthesis of iron oxide and gold/iron oxide nanoparticles. *J Nanosci Nanotechnol*. 2011;11:7214–7217.
3. Nguyen DT, Kim D-J, Kim K—S. Controlled synthesis and biomolecular probe application of gold nanoparticles. *Micron*. 2011;42: 207–227.
4. Sun C, Lee JSH, Zhang M. Magnetic nanoparticles in MR imaging and drug delivery. *Adv Drug Deliv Rev*. 2008;60:1252–1265.
5. Yoo DW, Lee J—H, Shin TH, Cheon J. Theranostic magnetic nanoparticles. *Acc Chem Res*. 2011;44:863–874.
6. Lou XW(D), Archer LA, Yang Z. Hollow micro-/nanostructures: Synthesis and applications. *Adv Mater*. 2008;20:3987–4019.
7. Caruso F, Spasova M, Susha A, Giersig M, Caruso RA. Magnetic nanocomposite particles and hollow spheres constructed by a sequential layering approach. *Chem. Mater*. 2001;13:109–116.
8. Huang Z, Tang F. Preparation, structure, and magnetic properties of mesoporous magnetite hollow spheres. *J Colloid Interface Sci*. 2005; 281:432–436.
9. Peng S, Sun S. Synthesis and characterization of monodisperse hollow Fe_3O_4 nanoparticles. *Angew Chem Int Ed*. 2007;46: 4155–4158.
10. Zeng HC. Ostwald ripening: A synthetic approach for hollow nanomaterials. *Curr Nanosci*. 2007;3:177–181.
11. Yang; HG, Zeng HC. Preparation of hollow anatase TiO_2 nanospheres via Ostwald ripening. *J Phys Chem B*. 2004;108:3492–3495.
12. Chang Y, Teo JJ, Zeng HC. Formation of colloidal CuO nanocrystallites and their spherical aggregation and reductive transformation to hollow Cu_2O nanospheres. *Langmuir*. 2005;21:1074–1079.
13. Hu P, Zhang X, Han N, Xiang W, Cao Y, Yuan F. Solution-controlled self-assembly of ZnO nanorods into hollow microspheres. *Cryst Growth Des*. 2011;11:1520–1526.
14. Lou XW, Wang Y, Yuan C, Lee JY, Archer LA. Template-free synthesis of SnO_2 hollow nanostructures with high lithium storage capacity. *Adv Mater*. 2006;18:2325–2329.
15. Liu S, Xing R, Lu F, Rana RK, Zhu J-J. One-pot template-free fabrication of hollow magnetite nanospheres and their application as potential drug carriers. *J Phys Chem C*. 2009;113:21042–21047.
16. Zhu L-P, Xiao H—M, Zhang W-D, Yang G, Fu S—Y. One-pot template-free synthesis of monodisperse and single-crystal magnetite hollow spheres by a simple solvothermal route. *Cryst Growth Des*. 2008;8:957–963.
17. Hu P, Yu L, Zuo A, Guo C, Yuan F. Fabrication of monodisperse magnetite hollow spheres. *J Phys Chem C*. 2009;113:900–906.
18. Cheng C, Xu F, Gu H. Facile synthesis and morphology evolution of magnetic iron oxide nanoparticles in different polyol processes. *New J Chem*. 2011;35:1072–1079.
19. Chen X, Zhang Z, Li X, Shi C. Hollow magnetite spheres: Synthesis, characterization, and magnetic properties. *Chem Phys Lett*. 2006; 422:294–298.
20. Fan T, Pan D, Zhang H. Study on formation mechanism by monitoring the morphology and structure evolution of nearly monodispersed Fe_3O_4 submicroparticles with controlled particle sizes. *Ind Eng Chem Res*. 2011;50:9009–9018.
21. Paul RC, Narula RC, Vasisht SK. Iron (Ill) acetates. *Transition Met Chem*. 1978;3:35–38.
22. Vasisht SK, Narula RC. Binuclear iron (III) acetates. *Transition Met Chem*. 1982;7:95–96.
23. Alivisatos AP. Naturally aligned nanoscrystals. *Science*. 2000;289: 736–737.
24. Pan DK, Zhang H, Fan T, Chen JG, Duan X. Nearly monodispersed core-shell structural Fe_3O_4@DFUR-LDH submicro particles for magnetically controlled drug delivery and release. *Chem Commun*. 2011; 47:908–910.
25. Cao S-W, Zhu Y-J, Chang J. Fe_3O_4 polyhedral nanoparticles with a high magnetization synthesized in mixed solvent ethylene glycol-water system. *New J Chem*. 2008;32:1526–1530.
26. Mitchell JA, Reid EE. The preparation of aliphatic amides. *J Am Chem Soc*. 1931;53:1879–1883.
27. Ratke L, Woorhes PW. Growth and Coarsening: Ostwald Ripening in Material Processing. New York: Springer; 2002.
28. Penn RL. Kinetics of oriented aggregation. *J Phys Chem B*. 2004; 108:12707–12712.

Manuscript received Feb. 4, 2013; and revision received Mar. 28, 2013.